Toward Safe Wearer-Prosthesis Interaction: Evaluation of Gait Stability and Human Compensation Strategy Under Faults in Robotic Transfemoral Prostheses

I-Chieh Lee, Ming Liu, *Member, IEEE*, Michael D. Lewek, Xiaogang Hu, *Senior Member, IEEE*, William G. Filer, and He Huang, *Senior Member, IEEE*

***Abstract*— Although advanced wearable robots can assist human wearers, their internal faults (i.e., sensors or control errors) also pose a challenge. To ensure safe wearer-robot interactions, how internal errors by the prosthesis limb affect the stability of the user-prosthesis system, and how users react and compensate for the instability elicited by internal errors are imperative. The goals of this study were to 1) systematically investigate the biomechanics of a wearer-robot system reacting to internal errors induced by a powered knee prosthesis (PKP), and 2) quantify the error tolerable bound that does not affect the user's gait stability. Eight non-disabled participants and two unilateral transfemoral amputees walked on a pathway wearing a PKP, as the controller randomly switched the control parameters to disturbance parameters to mimic the errors caused by locomotion mode misrecognition. The size of prosthesis control errors was systematically varied to determine the error tolerable bound that disrupted gait stability. The effect of the error was quantified based on the 1) mechanical change described by the angular impulse applied by the PKP, and 2) overall gait instability quantified using human perception, angular momentum, and compensatory stepping. The results showed that the error tolerable bound is dependent on the gait phase and the direction of torque change. Two balance recovery strategies were also observed to allow participants to successful respond to the induced errors. The outcomes of this study may assist the future design of an auto-tuning algorithm, volitionally-controlled powered prosthetic legs, and training of gait stability.**

Manuscript received 11 April 2022; revised 31 July 2022; accepted 1 September 2022. Date of publication 22 September 2022; date of current version 30 September 2022. This work was supported by the National Institutes of Health (NIH) under Grant EB024570. *(Corresponding author: I-Chieh Lee.)*

This work involved human subjects or animals in its research. Approval of all ethical and experimental procedures and protocols was granted by the Local Ethics Committee under Protocol No. 13-2689, and performed in line with the Declaration of Helsinki.

I-Chieh Lee, Ming Liu, Xiaogang Hu, and He Huang are with the Joint Department of Biomedical Engineering, University of North Carolina, Chapel Hill NC 27599 USA, and also with North Carolina State University, Raleigh, NC 27695 USA (e-mail: ichieh322@gmail.com; hhuang11@ncsu.edu).

Michael D. Lewek is with the Division of Physical Therapy, UNC Chapel Hill, Chapel Hill, NC 27599 USA.

William G. Filer is with the Department of Physical Medicine and Rehabilitation, UNC Chapel Hill, Chapel Hill, NC 27599 USA.

This article has supplementary downloadable material available at https://doi.org/10.1109/TNSRE.2022.3208778, provided by the authors.

Digital Object Identifier 10.1109/TNSRE.2022.3208778

***Index Terms*— Gait stability, machine fault, powered knee prosthesis, transfemoral amputee, user-prosthesis interaction.**

I. Introduction

IT IS impressive that humans can maintain consistent task performance reliably and repeatedly while encountering environmental uncertainty and internal movement variability and noise [1], [2], [3]. The ability to adapt to internal and external changes/errors has been discussed in many motor control theories [4], [5], [6] (e.g., minimize intervention principal [7]) where errors/changes that do not interfere with the task goal are tolerated by the individual. That is, the individual does not need to correct errors deemed insufficient to disrupt the task performance. It is of interest to know if this ability can be applied to a wearer-robot system. Technology has advanced to the point that wearable robotic limbs, such as robotic prosthetic legs, can be physically attached to humans to replace or augment the human biological limb function. Given that a wearer-robot system is often controlled by two independent mechanisms (human motor control system and machine controller), understanding how the wearer-robot system reacts and adapts to internal and/or external errors of the limb movement control becomes especially important to ensure safe wearer-robot interactions.

Specifically focusing on lower limb prosthetic legs, many studies have investigated the biomechanics of balance recovery of humans wearing a passive prosthesis while encountering external perturbations, such as, simulated uneven terrains in a virtual environment [8], [9], obstacle crossing [10], [11], unexpected external force impact on the pelvis [12], [13], prosthetic misalignment [14] that induce gait instability due to mechanical knee-buckling, altered frictional forces and mediolateral foot placement, or reduced toe clearance. These laboratory tasks elicited slips or trips by inducing *external* disturbances at specific gait phases and found that prosthetics users successfully adapted their walking strategy to compensate for external errors. Emerging robotic prostheses provide an exciting opportunity to restore the function of a missing limb, in terms of power production and intelligent control. However, these robotic devices are also subject to faults in sensors and control commands. For example, to enable seamless terrain transition for a robotic prosthesis, researchers have developed

a locomotion mode recognition system as a high-level prosthesis controller [15], [16], [17], [18], [19]. However, these systems occasionally experience sensor faults [20], [21] and decision errors (i.e., locomotion model [18], [22], [23], [24] or gait phase misrecognition [25], [26]), which causes intrinsic control errors in the prosthetic limbs. Therefore, advanced wearable robots, although capable of providing new functions to assist human wearers, also pose a new challenge to the wearer due to the potential creation of *internal* faults.

Several open questions therefore remain: 1) how does the internal error in the prosthesis limb affect the stability of the user-prosthesis system, and 2) how do human wearers react and compensate for the potential instability that is elicited by an internal error. Answering these questions is imperative to ensure the human wearer's safety, because a prosthesis control error might lead to falls and related injuries. By answering the first question, we potentially can characterize any internal errors and develop robust prosthesis controllers that allow wearers to tolerate any inadvertent faults. Answering the second question informs the potential human responses required to maintain balance during walking. Overall, addressing these knowledge gaps is critical for safe user-prosthesis interaction under the initial faults of robotic prostheses. Unfortunately, research in this area has been very limited.

For the first question, previous studies have reported that locomotion mode recognition systems for robotic prosthesis control have variable effects in the presence of classification errors, ranging from no effects to a disruption of the user's gait stability [18], [22], [23]. This observation motivated our team to investigate the effect of four types of terrain recognition errors when transitioning between level-ground and ramp walking on the human's stability [23]. The results showed that not all locomotion mode transition errors cause a user to report gait instability, and the effect of the errors depends on the type of mode misrecognition, the gait phase when the error occurs, and the error duration. That study implied that there may be a boundary of control error magnitude in different gait phases. Below the boundary, the user-prosthesis system can tolerate the error without experiencing gait instability, whereas an error above the boundary results in gait disruption. Identifying these boundaries could be important to develop a robust prosthesis controller that mimics the minimum intervention principle [27] in human motor control, (i.e., design a controller that only corrects an error that would interfere with task performance (outside the boundaries)). Unfortunately, the previous study [23] only investigated four types of locomotion mode misclassification errors, which is insufficient to identify such boundaries. For the second question, studying human reaction and compensation strategies resulting from external perturbations has been studied extensively on amputees who use passive or robotic prostheses [28]. However, to our knowledge, this topic has not been explored in response to intrinsic control errors of robotic prostheses.

Hence, the objectives of this study were to 1) quantify the error tolerable bound that does not affect the user's gait stability and 2) systematically investigate the biomechanics of wearer-robot systems reacting to internal errors induced by a robotic prosthetic leg. Different from our previous study [23], we created an experimental design to systematically scan the size of prosthesis control errors to determine the effects of those errors and the tolerable bound. A prosthesis control error simulator was designed to artificially create errors during stance phase that modulated the finite-state machine and impedance control of a powered prosthesis. We focused on stance phase only because prior work established that human wearers are more sensitive to prosthesis control errors during this phase [23]. The effects of the errors on the powered prosthesis and the gait stability of the wearer-robot system were evaluated. We expect that the results of this study could provide insight into wearer-robot interaction and reaction to intrinsic errors of robotic prosthesis and inform the future strategies to ensure the wearer's safety when walking with intelligent wearable robots.

II. Methods

A. Prosthetic Knee and Impedance Finite-State Control

We used a powered knee prosthesis (PKP) developed by our research group for this study. Sensors were embedded in the PKP to measure knee joint angle (potentiometer), knee joint angular velocity (encoder connected with the motor), and ground reaction force (GRF) (load cell, mini 58, ATI, NC, USA) mounted in line with the shank pylon). A multifunction data acquisition card collected all sensor measurements at 100 Hz and provided digital-to-analog control output to drive the DC motor through a motor controller (RE40, Maxon, Switzerland).

The PKP was controlled based on a finite-state impedance controller (IC) that is an established framework for robotic knee prosthesis control (Fig. 1). The gait cycle was divided into four phases based on the relationship between ground reaction force (GRF), knee angle(θ), and knee velocity($\dot{\theta}$) [29]: initial double support (IDS, m=1), single support (SS, m=2), swing flexion (SWF, m=3), and swing extension (SWE, m=4). The motion of the PKP was modulated by the knee joint torque (τ) that was generated based on a set of impedance parameters and the real-time knee joint angle (θ) and velocity ($\dot{\theta}$). Within each phase, three impedance parameters (IP), stiffness (K_m), equilibrium (θ_{em}) and damping (B_m) were set at constant (Equation 1). Thus, in total there are 12 IP (4 phases $*$ 3 parameters) that are needed to configure each locomotion mode.

$$\tau = K_m\left(\theta - \theta_{em}\right) + B_m * \dot{\theta} \tag{1}$$

B. Participants

Eight non-disabled participants (7 males and 1 female; age: 22.8 $\pm$ 2.6 years; height: 176.2 $\pm$ 2.9 cm; weight: 80.5 $\pm$ 7.1 kg) and two males with unilateral transfemoral amputation (TF01 age: 24 years; height: 168 cm; weight: 89 kg; Cause of Amputation: Congenital; TF02 age: 66 years; height: 166 cm; weight: 65 kg; Cause of Amputation: trauma with over 22 years post-amputation) were recruited in this study. All participants had no comorbidities, such as cardiovascular or neurological problems, that may affect their performance in this study. Subjects were informed of the research procedures and signed a written informed consent form to participant in

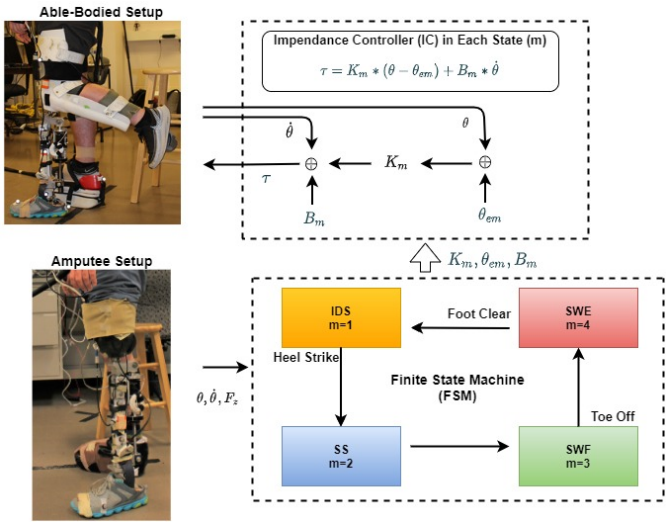

Fig. 1. Block diagram of powered knee prosthesis and impedance finite -state controller. Ground reaction force (Fz), knee joint angle (θ), and knee joint angular velocity ($\dot{\theta}$) are the direct measured from the PKP.

our protocol – approved by the Institutional Review Board of the University of North Carolina at Chapel Hill.

C. Human-Prostheses Configuration and Training

All participants were trained to walk with the PKP for at least five days (at least 15 hours). The purpose of the training was to ensure that all participants adapt to the PKP, were confident to walk with the device, and were able to produce a consistent gait cycle. All non-disabled participants wore an L-shaped bent-knee adaptor to connect the PKP to the bottom of the adaptor to create a human-prosthesis system. The prosthesis alignment was conducted based on the L.A.S.A.R. guidelines [30], and a height-adjustable shoe was used on the contralateral side for leveling the height of the hips. During training, the desired knee impedance parameters for each locomotion mode were calibrated for each participant by an experienced experimenter. After training, all non-disabled participants fit the criteria as high functional K3 level amputee that had the ability to ambulate independently with variable cadence.

Participants revisited the lab twice to complete the experimental protocol. They were asked to wear the PKP and walk on an 8 m pathway with a fall-arrest harness and handrails on both sides for protection. The first visit was to determine the level ground IP and customize the disturbance IPs that simulated the PKP error. The level ground IP was tuned using the reinforcement learning based impedance tuning framework developed by our team [31]. A tuning policy acts to adjust impedance parameters, according to the state of the human-prosthesis system. The IP were updated every four gait cycles until the knee angle of the PKP varied within a boundary (± 2 degrees) of the target knee angle profile. Tuning stopped when the participant could walk with the tuned IP to perform at least eight consistent knee motions (see Fig. 2A for tuned and targeted knee angle profile).

TABLE I
RATED SCORE FOR SUBJECTIVE EVALUATION OF GAIT INSTABILITY

Scores	Perceived level of gait instability
0	I did not feel any error
1	I perceived the error but still felt stable
2	I felt unstable but I can recover
3	I felt unstable and would fall

Errors in this study were imposed on the prosthetic knee joint by switching the level ground IPs to disturbance IPs. The mismatch of IPs mimicked the recognition errors associated with switching terrain, and added a pulse of error torque via the knee controller. The error in this study is characterized by 1) the magnitude of errors that corresponded to the perceived gait instability and 2) the onset timing of the error in a gait cycle. We investigated the machine errors only during stance phases (IDS and SS) because errors during these phases have a larger influence on balance stability compared to errors induced during swing [23]. We fixed the error pulse duration to 200 msec and only varied the torque magnitude to change the error size. The selection of 200 msec is based on our previous studies that reported the continuous misclassification in human intent generally lasted no more than 300 msec and 200 msec was enough to cause gait instability [23]. Error sizes were scored based on the presence of small (score 1), medium (score 2), and large (score 3) disturbances, based on each participant's reported level of gait instability (see Table I).

D. Approach to Determine the Disturbance Impedance Parameters

Considering that any IP that deviated from the current locomotion mode can be regarded as an error, the selection of disturbance IPs are infinite. To simplify the selection as well as ensure that the disturbance IP might actually be used in a real situation, the disturbance IP can be denoted as:

$$K_{dist} = \alpha\,(\Delta K * W) + K_{level} \tag{2}$$

$$\theta_{dist} = \alpha\,(\Delta\theta) + \theta_{level} \tag{3}$$

$$B_{dist} = \alpha\,(\Delta B * W) + B_{level} \tag{4}$$

where the $\boldsymbol{K_{level}}$, $\boldsymbol{\theta_{level}}$, and $\boldsymbol{B_{level}}$ are the IP customized for the participant on level ground walking, the $\boldsymbol{K_{dist}}$, $\boldsymbol{\theta_{dist}}$, and $\boldsymbol{B_{dist}}$ are the disturbance IP, W is the participant's body weight, $\boldsymbol{\alpha}$ is the weighting to scale the amplitude of disturbance level.

To determine the $\boldsymbol{\Delta K}$, $\boldsymbol{\Delta\theta}$, and $\boldsymbol{\Delta B}$, five sets of IPs tuned for transfemoral amputees on ramp ascent and ramp descent walking were used. The mean of $\boldsymbol{\Delta}$IP between level ground and ramp ascent/ramp descent modes were calculated in which $\boldsymbol{\Delta K}$ and $\boldsymbol{\Delta B}$ were normalized to the amputees' body weight. Thus, the relationship amount $\boldsymbol{\Delta K}$, $\boldsymbol{\Delta\theta}$, and $\boldsymbol{\Delta B}$ are fixed and corresponded to the ramp ascent or descent (values are shown in Appendix Table I). Therefore, the disturbance IP can be generated by assigning an $\boldsymbol{\alpha}$ value to equation 2, 3 and 4.

Since the amount of mechanical change elicited by disturbance IPs is unknown, the magnitude of error is estimated using angular impulse around the knee joint because it reflects shifts in both kinetics and kinematics when errors happen. Several sets of disturbance IPs were calculated by assigning $\boldsymbol{\alpha}$ from -10 to 10. The level ground IP, disturbance IPs, the mean θ and mean $\dot{\theta}$ from eight gait cycles were applied to equation 1 to estimate the change of angular impulse ($\boldsymbol{\Delta L}$). The change of angular impulse is defined as:

$$\Delta \boldsymbol{L} = \boldsymbol{L}_{\boldsymbol{error}} - \boldsymbol{L}_{\boldsymbol{level}} = \int_{t1}^{t2} \boldsymbol{\tau}\,(\boldsymbol{t})\boldsymbol{dt} - \int_{t1}^{t2} \boldsymbol{\tau}_{\boldsymbol{level}}\,(\boldsymbol{t})\boldsymbol{dt} \quad (5)$$

wherein t1 and t2 are 200 msec when an error starts and ends at the phase of IDS and SS, respectively; $\boldsymbol{\tau}\,(\boldsymbol{t})$ is the error torque applied to the knee joint; $\boldsymbol{\tau}_{\boldsymbol{level}}\,(\boldsymbol{t})$ is the knee torque recorded from the previous step at the same timing without error.

Note that negative $\boldsymbol{\Delta K}$ and $\boldsymbol{\Delta B}$ could result in negative K_{dist} and B_{dist} that violates the physical principal of the spring - damping system. These negative K_{dist} and B_{dist} were replaced with a zero and limited the magnitude of positive $\boldsymbol{\Delta L}$ provided to some participants in this study. The $\boldsymbol{\Delta L}$ **v.s.** $\boldsymbol{\alpha}$ curve provides a general estimation about the magnitude of the error inducing by the disturbance IP. To shorten the time to determine the disturbance IPs, a pilot test on two non-disabled participants was conducted to obtain the reference values of $\boldsymbol{\Delta L}$ in which participants reported small and large gait instability caused by the errors (see Fig. 2B).

The $\boldsymbol{\Delta L}$ **v.s.** $\boldsymbol{\alpha}$ curve and reference values of $\boldsymbol{\Delta L}$ were then used to determine the disturbance IPs expected to induce small, medium, and large gait instability. The disturbance IPs were systematically tested on each participant by increasing or decreasing by $0.2\boldsymbol{\Delta L}$ starting from the references $\boldsymbol{\Delta L}$. While participants walked on a 8 m pathway, the level ground IPs were switched randomly to the disturbance IP for 200 msec during one of the gait cycles. To ensure the participants could differentiate the source of gait instability, they were asked to identify the step where error was induced. The small and large disturbance IPs were determined when the participant scored the gait instability as 1 and 3, respectively. The mean $\boldsymbol{\Delta L}$ of small and large disturbance IPs was then taken as the reference values to determine the medium disturbance IPs. The systematic testing stopped when the participant scored the error as 2. Fig. 2 illustrates the procedure for determining the disturbance IPs.

In total, there were up to 24 disturbance IPs determined for 2 phases (IDA and SS) X 2 modes (ramp ascent and descent $\boldsymbol{\Delta}$IP) X 3 sizes (Small, Medium and Large disturbances) X 2 directions (positive and negative impulse). Zeroing of $\boldsymbol{K_{dist}}$ and $\boldsymbol{B_{dist}}$ limits the magnitude of the positive impulse. Therefore, three participants did not intervene during four conditions: IPs for medium and large negative impulse at 2 phases generated from ramp descent. These conditions were replaced by small disturbance IPs.

E. Data Collection

All data were collected on the 2nd visit. The participants wore the PKP to walk on an 8m pathway at a self-selected walking speed. Fifteen 3D Inertial Measurement Unit (IMU) sensors (MTw Awinda, Xsens, USA), setting a rigid body model with 12 or 13 segments, were used to obtain the kinematics for head, trunk, upper arms, forearms, upper legs, prosthetic lower leg, prosthetic feet, participants' shank, participants' feet, and the segments that supported by the L-shaped socket for non-disabled. During walking, the controller switched the level ground IP to the disturbance IP at the targeted gait phase with 200 msec duration during a randomly selected gait cycle. The mismatch of IP induced an error to the human-machine system. The order of conditions for 2 ramp $\boldsymbol{\Delta}$IP and 2 phases were counterbalanced, and the 3 error sizes and $\pm\boldsymbol{\Delta L}$ were randomized within a trial. Each condition was repeated 7 times, resulting in 168 disturbances for each participant. Rest periods were allowed between trials to avoid fatigue.

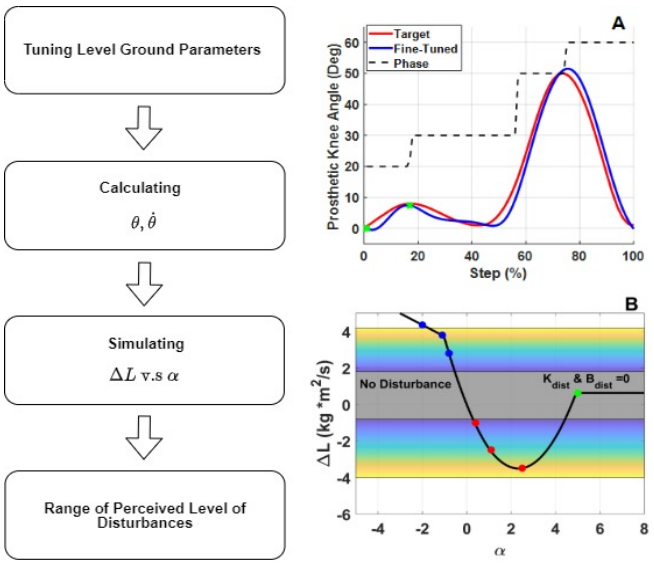

Fig. 2. Schematic illustration of the procedure for determining disturbance IPs. (2A) An example of the RL-based impedance tuning for the PKP system within the FSM framework. The red line is the targeted prosthetic knee angle. Blue line is the fine-tuned prosthetic knee angle averaged from 8 gait cycles. Black dash line is the phase in the FSM. The two green dots are the starts of IDS and SS phases where the knee angle and knee angular velocity were taken to estimate the angular impulse. (2B) An example to determine the disturbance IPs. Black line is the $\boldsymbol{\Delta L}$ **v.s.** $\boldsymbol{\alpha}$ curve. The color map indicates the reference range of $\boldsymbol{\Delta L}$ causing the feeling of small and large gait instability from the pilot testing. Red and blue dots mark the determined disturbance IPs where participant 1 reported small, medium, and large disturbances during the systematical testing. Green dot marks the $\boldsymbol{\alpha}$ value where increasing $\boldsymbol{\alpha}$ results in negative K_{dist} and B_{dist} and needs to replace K_{dist} and B_{dist} to zero.

F. Evaluation of Mechanical Change and Gait Instability

The effect of errors on gait instability was evaluated both subjectively and objectively. After walking to the end of the pathway, participants were asked to report a score regarding any perceived gait instability based on a four-scale questionnaire (see Table I). If the disturbance was rated larger than 2, the error was considered to cause gait instability.

To quantify the safety boundary, the mean of $\boldsymbol{\Delta L}$ from errors that received a perceived gait instability score $= 2$ was

reported. The mean change of prosthetic knee angle was also calculated using equation 6.

$$\boldsymbol{\Delta\ knee\ angle} = \frac{\int_{t1}^{t2} \boldsymbol{knee}_{error}\,(t) - \int_{t1}^{t2} \boldsymbol{knee}_{level}\,(t)}{t2 - t1} \tag{6}$$

wherein t1 and t2 are 200 msec when an error starts and ends, $\boldsymbol{knee}_{error}$ is the knee joint angle of the prosthetic step in which the error was induced; $\boldsymbol{knee}_{level}$ is the knee joint angle of the previous prosthetic step at the same gait cycle timing. $\boldsymbol{\Delta\ knee\ angle}$ indicates the deviation from normative knee angle due to error (": +" knee flexion and ":-" extension)

Whole-body angular momentum (H) about the whole-body center of mass (COM) was used as an objective measurement of gait stability. Joint positions and segment angular velocities were low-pass filtered using a 4th-order Butterworth filter with a 6 Hz cut off frequency. The rigid body model was used to calculate the participant's whole-body COM and angular momentum. The head was modeled as a sphere, and the other segments were modeled as cylinders. Anthropometric measurements included body weight, height, and segment lengths were taken from each participant to accurately reconstruct the representative model. For each segment, including the powered knee prosthesis, the COM location, the radius of the mid-, proximal, and distal radii of the other segments were estimated based on the anthropometric dimension of the 50 percentile composite subjects from Hanavan [32]. The segment mass for each participant was calculated as a percentage of whole-body mass based on Leva [33], and the mass of the prosthetic foot and shank were measured. The whole-body angular momentum ($\vec{H}$), was calculated as the sum of each individual segment's angular momentum about the whole-body COM from the global frame of reference as:

$$\vec{H} = \sum_{i=1}^{13} [\left(\vec{P}_{CM}^{\,i} - \vec{P}_{CM}\right) \times m_i \left(\vec{V}_{CM}^{\,i} - \vec{V}_{CM}\right) + \overleftrightarrow{I}^{\,i}\,\vec{\omega}^{\,i}] \tag{7}$$

where $\vec{P}_{CM}^{\,i}$ and $\vec{V}_{CM}^{\,i}$ is the position and velocity of ith segment's COM position and velocity. $\vec{P}_{CM}$ and $\vec{V}_{CM}$ is the position and velocity of the whole-body COM's position and velocity. m_i is the mass of the ith segment. $\overleftrightarrow{I}^{\,i}$ and $\vec{\omega}^{\,i}$ are the segments' inertia tensor (3×3) and angular velocity about the segment's COM, respectively. All the variables were calculated with respect to the global reference frame.

It is known that IMU-based motion tracking has a drift of the estimated orientation over time due to the gyroscope bias and non - homogeneous magnetic field, especially in indoor buildings. To correct the drift, we applied a simple solution by rotating the $\vec{H}$ with respect to the orientation of the pelvis sensor to align the y-axis pointing in the walking direction (anterior-posterior direction). We selected the pelvis sensor because it is close to the whole-body center of mass, which is relatively stable, to represent the orientation of walking direction.

The rotation from segment to global frame of reference was given from the Xsens file using the quaternion vector (q0, q1, q2, q3) with q0 as a real value and q1, q2 and q3 as complex numbers. Hence, we can calculate the rotation matrix (R_{GP}) describing the orientation of the pelvis segment as:

$$R_{GP} = \begin{bmatrix} 1 - 2q_2^2 - 2q_3^2 & 2q_1q_2 - 2q_0q_3 & 2q_1q_3 - 2q_0q_2 \\ 2q_1q_2 - 2q_0q_3 & 1 - 2q_1^2 - 2q_3^2 & 2q_2q_3 - 2q_0q_1 \\ 2q_1q_3 - 2q_0q_2 & 2q_2q_3 - 2q_0q_1 & 1 - 2q_1^2 - 2q_2^2 \end{bmatrix} \tag{8}$$

The rotation of $\vec{H}$ from global to pelvis orientation can be denoted as:

$$\vec{H}_{PG} = \vec{H} \times R_{GP}^{T} \tag{9}$$

where ${R_{GP}}^T$ is the transpose of R_{GP}, $\vec{H}$ is angular momentum from global frame of reference and the $\vec{H}_{PG}$ is the rotated angular momentum from global to pelvis frame of reference. Because the PKP errors would cause the irregular knee flexion or extension, the full-body angular momentum in the sagittal plane (": + " posterior and ": - " anterior) was used.

The peak magnitude of anterior angular momentum (-|H|) was calculated to quantify the error that resulted from irregular knee flexion, and the magnitude of posterior angular momentum (+|H|) was calculated to quantify the error resulting from irregular knee extension. To reduce the variation between participants, H was normalized in a dimensionless form divided by the participant's weight, height, and average walking speed.

Step length and width were calculated using the position of the prosthetic heel and intact heel to evaluate if the participant regulated these gait parameters as a compensation strategy to recover gait balance. The ground reaction force (GRF) was used to investigate if the participant applied a strategy to avoid the error by delaying the loading of body weight on the prosthetic leg. Delayed loading was defined as the GRF of the prosthetic leg being less than 40% of body weight during the initial 200 msec of the gait cycle. The angular momentum of the trunk and intact leg during the stance phase were also calculated to investigate the regulation of whole-body angular momentum.

G. Statistical Analysis

Correlation analyses were performed to investigate the error effects on mechanical change and gait instability. Due to non-normal and heteroscedastic data distributions, Spearman's rank correlation coefficient was performed. Correlation between |H| and $\Delta kneeangle$ was tested to investigate if the change of prosthesis knee angle propagated to the whole - body level and influenced the overall gait instability. The potential correlation between magnitude of |H| and step length/width was tested to investigate if gait instability led to a compensatory step associated with an increased base of support. The significance level was set as $\alpha = 0.05$.

III. Results

A. Effect of the Estimated Error Size

Fig. 3 demonstrates two representative trials when an error was induced during the SS phase for 200 msec. When the error was applied, the knee angle deviated from the normal knee motion. The large negative (-2.40 kg*m^2/s) and positive (6.88 kg*m^2/s) change of angular impulse ($\boldsymbol{\Delta L}$) within the 200 msec period caused knee flexion and extension respectively, resulting in the rated gait instability of 3.

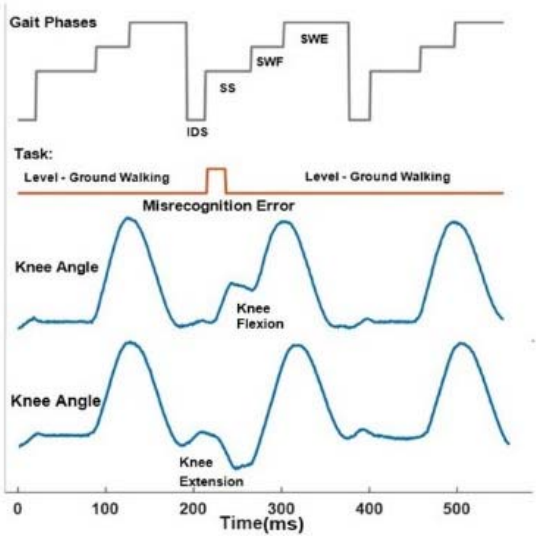

Fig. 3. Two representative trials from participant 4 when the error occurred at the SS phase for 200 msec. Phase "1-4" represents IDS, SS, SWF, and SWE, respectively. The red line indicates the timing that the error was applied. The large negative and positive $\Delta \boldsymbol{L}$ caused knee flexion and extension, respectively, resulted in the rated gait instability of 3.

B. Mechanical Changes on Angular Impulse (Safety Bound)

Fig. 4 and table II shows the mean change of mechanical impulse ($\boldsymbol{\Delta L}$) that occurred with a gait instability rating of 2 for each participant. The magnitude of mechanical impulse change caused by the critical errors varied across different gait phases and participants. At the initial double support phase (IDS), a larger amount of positive ΔL (extension impulse) on was required for participants to perceive gait instabilities compared to error induced negative impulse (flexion impulse). At the single support phase (SS), participant 1,3, 5, 7, TF01, and TF02 required more negative impulse to perceive gait instability.

C. Angular Momentum

Fig. 5A - 5D show the trace of H from a representative participant as they rated gait instability from 1 to 3. In both cases, the change of irregular knee flexion / extension showed a significant moderate correlation with the magnitude of anterior/posterior |H| (IDS Knee Flexion Errors: $\rho_s < -0.212$, $p_s < 0.001$; SS Knee Flexion Errors: $\rho_s < -0.207$, $p_s < 0.001$; SS Knee Extension Errors: $\rho_s < -0.233$, $p_s < 0.001$). For errors applied during the IDS phase, the correlation between irregular knee extension and the peak value of posterior |+H| was not significant (IDS Knee Extension Errors: $\rho = -0.114$, $p = 0.06$). By examining each individual in the non-disabled group, we found the traces of H demonstrated a double oscillation pattern in some trials. This pattern was distinct from other types of errors and occurred for non-disabled participant 2 (57%), 4 (55%), 5 (65%), 6 (45%), and 7 (38%) within all the cases rated with instability scores ≥2 (see Fig. 5C). In addition, the results of mean anterior and posterior peak $|\boldsymbol{H}|$ demonstrated a lower magnitude change in the amputee group compared to non-disabled group (see Fig. 5E).

For the errors that caused gait instability ≥2, the correlation between the H and trunk angular momentum during the stance phase was calculated. A strong to medium positive correlation was found in the non-disabled group and TF 02 (TF02 (R^2): IDS Flexion Error: 0.56; IDS Extension Error: 0.38; SS Flexion Error: 0.47; SS Extension Error: 0.36; Non-disabled (R^2): IDS Flexion Error: 0.55 ± 0.24; IDS Extension Error: 0.40± 0.17; SS Flexion Error: 0.46± 0.13; SS Extension Error: 0.47± 0.12). However, no significant correlation was found in TF01. Fig. 6B shows that TF01 controlled the trunk angular momentum close to zero and was not perturbed by the errors. In addition, we also observed that the angular momentum of the intact leg demonstrated a faster change from posterior to anterior to compensate for the oscillation of whole-body angular momentum in both groups (See Fig. 6A).

D. Compensatory Steps, and Ground Reaction Force

Participant's step length and step width were highly variable and showed weak or no significant correlation between the peak anterior and posterior H and step length and width in both groups. A weak significant correlation was found that the participants had the tendency to increase step width when errors were applied at IDS resulted in irregular knee extension (Step width: $\rho = 0.12$, $p = 0.016$) and increase both step width and length when errors applied at SS resulted in irregular knee flexion (Step width : $\rho = 0.144$, $p = 0.007$; Step Length $\rho = 0.213$, $p < 0.001$:). From the GRF data, we found that three out of eight participants in the non-disabled group hesitated to load their body weight on the PKP. Fig. 7 illustrates a case that the ground reaction force was less than 40% of the participant's body weight during the initial 200 msec of the gait cycle. The percentage of such an occurrence within all the error cases was 14.88% for participant 4, 7.14% for participant 6, and 8.93% for participant 7.

IV. Discussion

This study aims to investigate the biomechanics of wearer-robot interaction in responding to the errors applied by a powered prosthetic leg and identify the safety boundary of errors that impact the safe and confident use of powered artificial legs. The effects of errors due to unmatched impedance parameters was quantified based on 1) mechanical change described using angular impulse, and 2) overall gait instability quantified using human perception and angular momentum.

Inspired by the minimize intervention principle (MIP) in human motor control [27], a different perspective was taken in this study to investigate the effect of machine errors in the wearer-robot system. It is common that most wearer-robot studies consider errors as failure to the system and aim to pursue a higher accuracy rate or methods to correct the errors (i.e., increase the accuracy of terrain recognition for the volitional controller of powered artificial legs [10], [11], [12], [13], [14], [15], [16], [17]. Instead of regarding all errors are "harmful", instead we have relied on the user's feedback to estimate a safety boundary for errors that would not affect gait stability during level-ground walking. Following

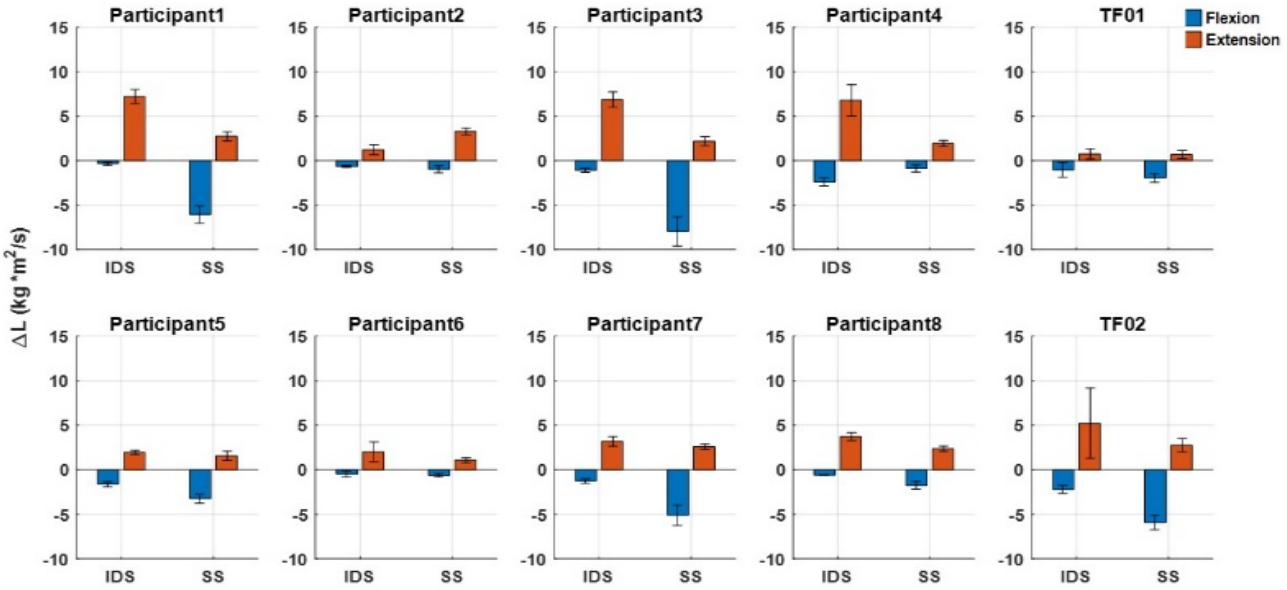

Fig. 4. Change of angular impulse at the prosthetic knee joint caused rated scores of gait instability to 2 on two phases for each participant. These values indicate the safety boundary for the participants.

TABLE II
MEAN AND STANDARD DEVIATION OF CHANGE OF ANGULAR IMPULSE AT THE PROSTHETIC KNEE JOINT CAUSED RATED SCORES OF GAIT INSTABILITY TO 2 ON TWO PHASES FOR EACH PARTICIPANT

	IDS		SS	
	Flexion	**Extension**	**Flexion**	**Extension**
Participant1	-0.32±0.16	7.24±0.79	-6.05±0.98	2.74±0.51
Participant 2	-0.64±0.13	1.23±0.57	-0.95±0.39	3.3±0.38
Participant3	-1.08±0.21	6.89±0.86	-7.95±1.63	2.20±0.49
Participant4	-2.40±-0.45	6.80±1.76	-0.86±0.41	1.94±0.34
Participant5	-1.61±0.28	1.96±0.22	-3.24±0.52	2.15±0.53
Participant6	-0.47±0.34	2.02±1.11	-0.63±0.20	1.07±0.27
Participant7	-1.26±0.24	3.19±0.53	-5.10±-1.14	2.58±0.32
Participant8	-0.588±0.05	3.73±0.44	-1.75±0.43	2.36±0.29
TF01	-1.02±0.83	0.97±-0.48	-1.95±0.50	0.70±0.45
TF02	-2.20±0.45	5.24±3.93	-5.93±0.80	2.76±0.75

the MIP, given errors within this bound would not interfere with task performance, and thus the prosthesis control can be designed to intervene only when the error may elicit physical instability (i.e., outside the bound). This approach could reduce the number of error corrections, simplify the design of control systems, and minimize the control-dependent noise while maintaining the safety and robustness of the controller. Moreover, the estimated safety boundary from our proposed experimental protocol could be applied to auto-tune the control parameter of the powered prosthetic leg [34], [35], [36]. During the tuning process, the control parameters will update after every few steps, and the estimated angular impulse can be set as the bound of the update interval for the next control parameters. Thus, the change of control parameters during tuning would not induce a large disturbance to the prosthetic user and could make the tuning safer.

It is noted that the estimated safety boundary quantified by the change of angular impulse at the knee joint is dependent on the gait phase, the direction of torque change, and was varied across participants (Fig. 4). This might be due to individuals having different levels of demand for balance [37], [38]. Firstly, some participants showed a smaller error-tolerant range (TF01, participant 2 and 6) compared to other participants. These participants might be particularly sensitive to errors and felt threatened even when the PKP performed a small, unexpected changes. Secondly, a small change of *negative* impulse (knee flexion torque) during the IDS phase was enough for all participants to report gait disturbance compared to the SS phase, and a small *positive* impulse change (knee extension torque) during the SS phase compared to the IDS phase contributed to 5 out of 8 non-disabled participants and one amputee (TF02) reporting gait instability. This result indicates

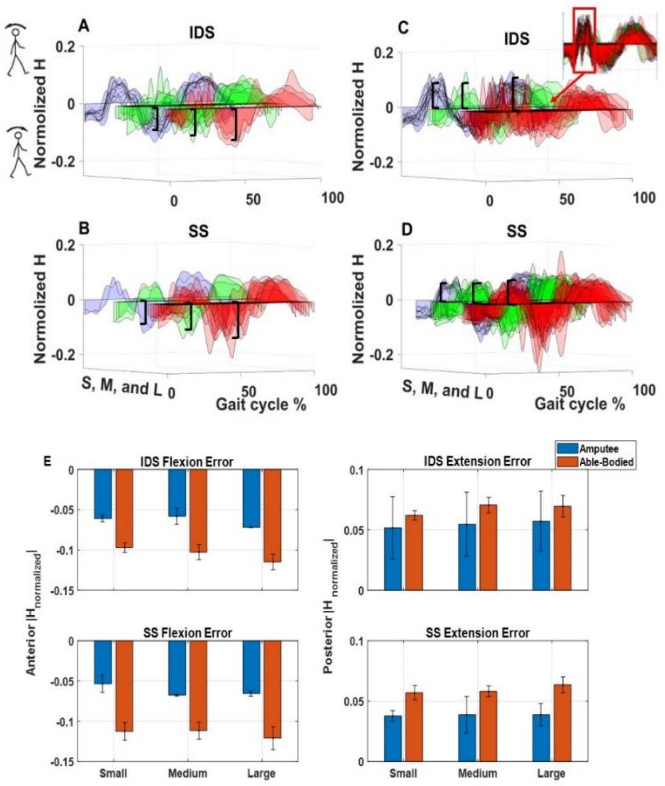

Fig. 5. Resultant whole-body and intact leg angular momentum in the sagittal plane. Fig. A - D demonstrated the traces of H from participant 4 when the errors applied at the IDS caused knee flexion (5A), at the SS caused knee flexion (5B), at the IDS caused knee extension (5C), and at the SS causing knee extension (5D). The red, green, and blue lines indicate the rated gait instability as 3 (L), 2 (M) and 1(S), respectively. The black brackets mark the average range of H peaks. A projection view of H versus time is also provided for Fig. 5C as an aside to better illustrate the distinct pattern of H. The red rectangle highlights the difference in peaks. Fig. 5E shows the mean anterior and posterior peak $|\boldsymbol{H}|$ when the applied errors caused knee flexion or knee extension for participants to report small, medium, and large gait instability, respectively.

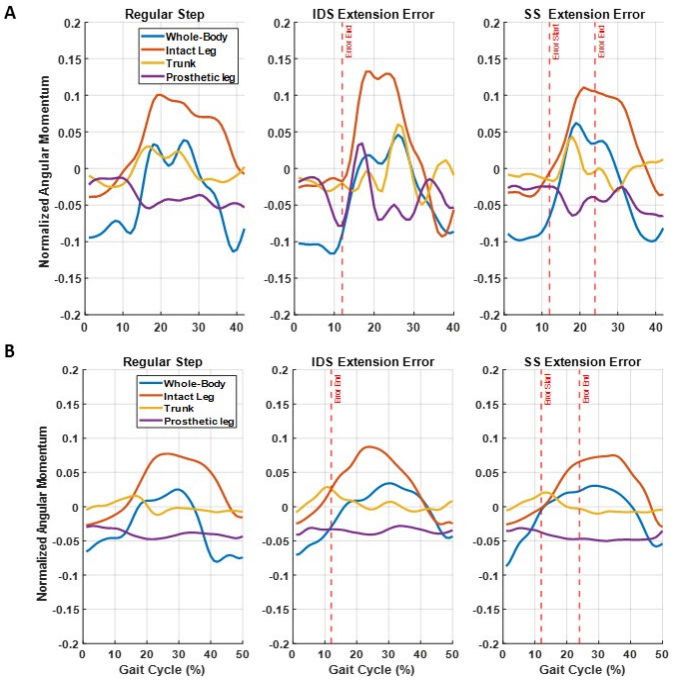

Fig. 6. (6A) A representative case of the whole-body, trunk, and intact leg angular momentum during the period from PKP heel contact to the intact heel contact for participants with strong correlation between trunk and whole-body angular momentum. (6B) A representative case of the whole-body, trunk, and intact leg angular momentum for TF01.

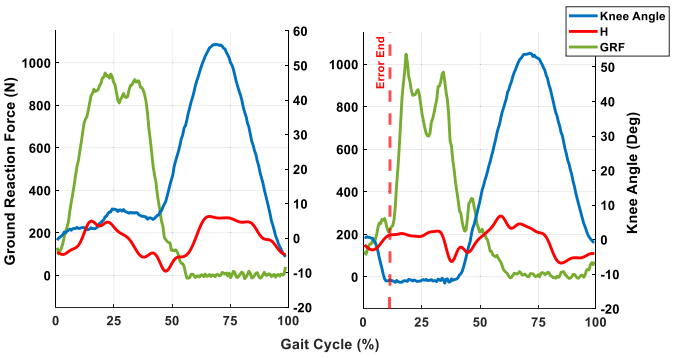

Fig. 7. Representative case for unloading body weight. Left panel demonstrates a regular gait cycle. Right panel shows that the error caused knee extension, but the delayed loading of body weight showed on the GRF resulted in small change of H.

that when the error induced torque change is consistent with the direction of knee flexion/extension angular change, a small change can lead to excessive movement and easily create the sensation of gait instability. This observation is consistent with the finding in [37] and [39], whereas slips begin later in the stance phase (SS in our case), a short and slower slip is enough to cause gait disturbance. The slip induced gait disturbance is similar to the error caused by knee extension torque in this study [40]. Since the error tolerant range is sensitive to the phase and direction of torque change, one can consider these two essential factors to carefully design the impedance parameters for each locomotion mode in each state, so that when errors occur, the resulting impulse change could still be within the safety boundary to alleviate the effect of error.

By investigating the biomechanics of wearer-robot interaction in response to errors, we observed some strategies that could be used for balance recovery or reduce the effect of machine error. As expected, in general, the knee flexion/extension error affects the whole-body level and showed a strong positive correlation between the peak of angular momentum (|H|) and mechanical change of knee angle (Fig. 5). In addition, the amputee group showed a smaller value of |H| compared to the non-disabled group (see Fig. 5E). This result aligns with previous studies that the magnitude of H reflects on the level of gait instability and the ability to sufficiently reduce the excessive change of H is crucial to avoid a fall [41], [42], [43], [44]. In this study, two strategies were observed to regulate H. When participants perceived a larger disturbance, they quickly swing the intact leg forward which resulted in a faster change of intact angular moment from posterior to anterior direction. In addition, participants who can maintain stable trunk angular momentum were able to restrain the normal patterns of H, such as TF01 [37], [39], [45] (see Fig. 6B) compared to other participants whose trunk angular momentum oscillated with H (see Fig. 6A). Moreover,

the distinct double oscillation pattern of H found in some non-disabled participants might indicate a correction was composed of a series of ballistic submovements (e.g., undershooting and overshooting) to counteract the effect of the error during a short period [46], [47] instead of applying one adjustment to regain stability (see Fig. 5C). It is unclear why these participants occasionally required multiple corrections and what the pros and cons are for this pattern with respect to maintaining gait stability.

From the ground reaction force data (see Fig. 6C), some participants slightly delayed their body weight loading (<200 msec) onto the PKP and successfully reduced the effect of the error that occurred during IDS to propagate to the whole-body level (small change in H was observed). This strategy could potentially avoid the terrain misrecognition errors for volitional control of powered leg prosthesis. If the controllers made a wrong decision in identifying the future terrain and switched the control parameters in the swing phase, the error due to mismatch of the control parameters could be alleviated or noticed by the users by delaying loading of body weight.

The compensation step length and width have no or weak association with |H|. One explanation may be multiple viable strategies are available such as 'skate -over' and 'walk-over' that have been reported previously [40]. These strategies alone could lead to disparate foot displacement, as the skate-over strategy allows carrying over the large anterior |H| to take a longer step, while the walk-over strategy quickly breaks the unpreferred rotation with an immediate, short step.

This study has a number of limitations. The error type in this study is associated with mode misrecognition, it is only a small subset of the possible internal errors that a prosthesis could exhibit. Different control approaches, such as volitional controllers or reflex-based controllers, may exhibit internal errors that are very different in nature than the ones described in this paper. We only studied the errors with a 200 msec duration since our previous study showed this is the shortest duration to affect balance and is suitable to investigate the safety boundary. However, it is unknown whether similar error durations will be observed. The repeated trials allowed us to expand the error samples and provide a longer exposure time for participants to adapt to the errors. However, users may adopt different gait strategies knowing that the device is likely to experience an error and may walk cautiously or be prepared to make balance recovery actions. As such, we cannot rule out the possibility that the compensatory actions seen in this study may not be fully representative of actions that may be taken in the real world. Given that the size and direction of errors were randomly provided, it prevents us from systematically studying the learning or adaptation process. Thus, further study could consider reducing the error types and directly conducting a learning study. Moreover, in this study, participants' feeling of gait instability was used to customize the error size. Note that some participants were more sensitive to error (small error-tolerant range in Fig. 4), and thus, even though the error did not disturb gait stability based on the measurement of whole-body angular momentum, they tended to interpret the error as a potential fall risk. Thus, further study could consider the factors that are directly related to the subjective perception of gait instability.

V. Conclusion

This study investigated the biomechanics of wearer-robot systems reacting to internal errors induced by a powered knee prosthesis, and quantified the error tolerable bound that does not affect the user's gait stability. Two balance recovery strategies: regulating trunk and intact leg angular momentum, and delaying the loading of body weight, were observed for participants to successful respond to machine errors. The error tolerable bound depends on the gait phases, the direction of torque change, and was variable across participants. The outcomes of this study could aid future design of an auto-tuning algorithm, volitionally-controlled powered prosthetic legs, and training of gait stability.

References

[1] N. Bernstein, *The Co-Ordination and Regulation of Movements*. Pergamon Press, 1967.

[2] N. A. Bernstein, *Dexterity and its Development*. London, U.K.: Psychology Press, 2014.

[3] A. A. Faisal, L. P. J. Selen, and D. M. Wolpert, "Noise in the nervous system," *Nature Rev. Neurosci.*, vol. 9, no. 4, pp. 292–303, 2008.

[4] M. L. Latash, J. P. Scholz, and G. Schöner, "Motor control strategies revealed in the structure of motor variability," *Exerc. Sport Sci. Rev.*, vol. 30, no. 1, pp. 26–31, Jan. 2002.

[5] E. Todorov and M. I. Jordan, "Optimal feedback control as a theory of motor coordination," *Nature Neurosci.*, vol. 5, no. 11, pp. 1226–1235, 2002.

[6] J. P. Cusumano and J. B. Dingwell, "Movement variability near goal equivalent manifolds: Fluctuations, control, and model-based analysis," *Hum. Movement Sci.*, vol. 32, no. 5, pp. 899–923, Oct. 2013.

[7] D. Liu and E. Todorov, "Evidence for the flexible sensorimotor strategies predicted by optimal feedback control," *J. Neurosci.*, vol. 27, no. 35, pp. 9354–9368, Aug. 2007.

[8] J. A. Sturk *et al.*, "Maintaining stable transfemoral amputee gait on level, sloped and simulated uneven conditions in a virtual environment," *Disab. Rehabil., Assistive Technol.*, vol. 14, no. 3, pp. 226–235, Apr. 2019.

[9] E. H. Sinitski, E. D. Lemaire, N. Baddour, M. Besemann, N. Dudek, and J. S. Hebert, "Maintaining stable transtibial amputee gait on level and simulated uneven conditions in a virtual environment," *Disab. Rehabil., Assistive Technol.*, vol. 16, no. 1, pp. 40–48, Jan. 2021.

[10] A. H. Vrieling *et al.*, "Obstacle crossing in lower limb amputees," *Gait Posture*, vol. 26, no. 4, pp. 587–594, Oct. 2007.

[11] C. T. Barnett, R. C. Polman, and N. Vanicek, "Longitudinal kinematic and kinetic adaptations to obstacle crossing in recent lower limb amputees," *Prosthetics Orthotics Int.*, vol. 38, no. 6, pp. 437–446, Dec. 2014.

[12] A. Olenšek, M. Zadravec, H. Burger, and Z. Matjačić, "Dynamic balancing responses in unilateral transtibial amputees following outward-directed perturbations during slow treadmill walking differ considerably for amputated and non-amputated side," *J. NeuroEng. Rehabil.*, vol. 18, no. 1, p. 123, Dec. 2021.

[13] M. J. Major, C. K. Serba, and K. E. Gordon, "Perturbation recovery during walking is impacted by knowledge of perturbation timing in below-knee prosthesis users and non-impaired participants," *PLoS ONE*, vol. 15, no. 7, Jul. 2020, Art. no. e0235686.

[14] N. J. Rosenblatt, A. Bauer, D. Rotter, and M. D. Grabiner, "Active dorsiflexing prostheses may reduce trip-related fall risk in people with transtibial amputation," *J. Rehabil. Res. Develop.*, vol. 51, no. 8, pp. 1229–1242, 2014.

[15] H. Huang, F. Zhang, L. J. Hargrove, Z. Dou, D. R. Rogers, and K. B. Englehart, "Continuous locomotion-mode identification for prosthetic legs based on neuromuscular–mechanical fusion," *IEEE Trans. Biomed. Eng.*, vol. 58, no. 10, pp. 2867–2875, Oct. 2011.

[16] H. Huang, T. A. Kuiken, and R. D. Lipschutz, "A strategy for identifying locomotion modes using surface electromyography," *IEEE Trans. Biomed. Eng.*, vol. 56, no. 1, pp. 65–73, Jan. 2009.

[17] D. Joshi and M. E. Hahn, "Terrain and direction classification of locomotion transitions using neuromuscular and mechanical input," *Ann. Biomed. Eng.*, vol. 44, no. 4, pp. 1275–1284, 2016.

[18] H. A. Varol, F. Sup, and M. Goldfarb, "Multiclass real-time intent recognition of a powered lower limb prosthesis," *IEEE Trans. Biomed. Eng.*, vol. 57, no. 3, pp. 542–551, Mar. 2010.

[19] A. J. Young, A. M. Simon, N. P. Fey, and L. J. Hargrove, "Intent recognition in a powered lower limb prosthesis using time history information," *Ann. Biomed. Eng.*, vol. 42, no. 3, pp. 631–641, 2014.

[20] H. Huang, F. Zhang, Y. L. Sun, and H. He, "Design of a robust EMG sensing interface for pattern classification," *J. Neural Eng.*, vol. 7, no. 5, Oct. 2010, Art. no. 056005.

[21] A. Dutta, K. Koerding, E. Perreault, and L. Hargrove, "Sensor-fault tolerant control of a powered lower limb prosthesis by mixing mode-specific adaptive Kalman filters," in *Proc. Annu. Int. Conf. IEEE Eng. Med. Biol. Soc.*, Aug./Sep. 2011, pp. 3696–3699.

[22] E. C. Martinez-Villalpando and H. Herr, "Agonist-antagonist active knee prosthesis: A preliminary study in level-ground walking," *J. Rehabil. Res. Develop.*, vol. 46, no. 3, pp. 361–373, 2009.

[23] F. Zhang, M. Liu, and H. Huang, "Effects of locomotion mode recognition errors on volitional control of powered above-knee prostheses," *IEEE Trans. Neural Syst. Rehabil. Eng.*, vol. 23, no. 1, pp. 64–72, Jan. 2015.

[24] F. Zhang, M. Liu, and H. Huang, "Investigation of timing to switch control mode in powered knee prostheses during task transitions," *PLoS ONE*, vol. 10, no. 7, Jul. 2015, Art. no. e0133965.

[25] C. Karakasis and P. Artemiadis, "Real-time kinematic-based detection of foot-strike during walking," *J. Biomech.*, vol. 129, Dec. 2021, Art. no. 110849.

[26] X. Jiang, K. Chu, M. Khoshnam, and C. Menon, "A wearable gait phase detection system based on force myography techniques," *Sensors*, vol. 18, no. 4, p. 1279, Apr. 2018.

[27] E. Todorov and M. Jordan, "A minimal intervention principle for coordinated movement," in *Proc. Adv. Neural Inf. Process. Syst.*, vol. 15, 2002, pp. 1–8.

[28] F. Zhang, S. E. D'Andrea, M. J. Nunnery, S. M. Kay, and H. Huang, "Towards design of a stumble detection system for artificial legs," *IEEE Trans. Neural Syst. Rehabil. Eng.*, vol. 19, no. 5, pp. 567–577, Oct. 2011.

[29] M. Liu, F. Zhang, P. Datseris, and H. Huang, "Improving finite state impedance control of active-transfemoral prosthesis using dempster-shafer based state transition rules," *J. Intell. Robot Syst.*, vol. 76, nos. 3–4, pp. 461–474, Dec. 2014.

[30] M. Bellmann, S. Blumentritt, M. Pusch, T. Schmalz, and M. Schonemeier, *The 3D LASAR—A New Generation of Static Analysis for Optimising Prosthetic and Orthotic Alignment*. Dortmund, Germany: Verlag Orthopädie-Technik, 2017.

[31] M. Li, Y. Wen, X. Gao, J. Si, and H. Huang, "Toward expedited impedance tuning of a robotic prosthesis for personalized gait assistance by reinforcement learning control," *IEEE Trans. Robot.*, vol. 38, no. 1, pp. 407–420, Feb. 2021.

[32] E. P. Hanavan, Jr., "A mathematical model of the human body," Air Force Aerosp. Med. Res. Lab, Wright-Patterson AFB, OH, USA, Tech. Rep. AFIT-GA-PHYS-64-3, 1964.

[33] P. de Leva, "Adjustments to Zatsiorsky–Seluyanov's segment inertia parameters," *J. Biomech.*, vol. 29, no. 9, pp. 1223–1230, Sep. 1996.

[34] H. Huang, D. L. Crouch, M. Liu, G. S. Sawicki, and D. Wang, "A cyber expert system for auto-tuning powered prosthesis impedance control parameters," *Ann. Biomed. Eng.*, vol. 44, no. 5, pp. 1613–1624, May 2016.

[35] Y. Wen, M. Li, J. Si, and H. Huang, "Wearer-prosthesis interaction for symmetrical gait: A study enabled by reinforcement learning prosthesis control," *IEEE Trans. Neural Syst. Rehabil. Eng.*, vol. 28, no. 4, pp. 904–913, Apr. 2020.

[36] M. Li, X. Gao, Y. Wen, J. Si, and H. H. Huang, "Offline policy iteration based reinforcement learning controller for online robotic knee prosthesis parameter tuning," in *Proc. Int. Conf. Robot. Autom. (ICRA)*, May 2019, pp. 2831–2837.

[37] C. M. Rasmussen and N. H. Hunt, "Unconstrained slip mechanics and stepping reactions depend on slip onset timing," *J. Biomech.*, vol. 125, Aug. 2021, Art. no. 110572.

[38] R. Ferber, L. R. Osternig, M. H. Woollacott, N. J. Wasielewski, and J.-H. Lee, "Reactive balance adjustments to unexpected perturbations during human walking," *Gait Posture*, vol. 16, no. 3, pp. 238–248, Dec. 2002.

[39] B. E. Moyer, M. S. Redfern, and R. Cham, "Biomechanics of trailing leg response to slipping—Evidence of interlimb and intralimb coordination," *Gait Posture*, vol. 29, no. 4, pp. 565–570, Jun. 2009.

[40] T. Bhatt, J. D. Wening, and Y.-C. Pai, "Influence of gait speed on stability: Recovery from anterior slips and compensatory stepping," *Gait Posture*, vol. 21, no. 2, pp. 146–156, Feb. 2005.

[41] M. Pijnappels, M. F. Bobbert, and J. H. V. Dieën, "Push-off reactions in recovery after tripping discriminate young subjects, older non-fallers and older fallers," *Gait Posture*, vol. 21, no. 4, pp. 388–394, Jun. 2005.

[42] J. Begue, N. Peyrot, G. Dalleau, and T. Caderby, "Age-related changes in the control of whole-body angular momentum during stepping," *Exp. Gerontol.*, vol. 127, Nov. 2019, Art. no. 110714.

[43] R. C. Sheehan, E. J. Beltran, J. B. Dingwell, and J. M. Wilken, "Mediolateral angular momentum changes in persons with amputation during perturbed walking," *Gait Posture*, vol. 41, no. 3, pp. 795–800, Mar. 2015.

[44] A. K. Silverman and R. R. Neptune, "Differences in whole-body angular momentum between below-knee amputees and non-amputees across walking speeds," *J. Biomech.*, vol. 44, no. 3, pp. 379–385, Feb. 2011.

[45] H. Herr and M. Popovic, "Angular momentum in human walking," *J. Exp. Biol.*, vol. 211, pp. 467–481, Feb. 2008.

[46] D. E. Meyer, J. K. Smith, S. Kornblum, R. A. Abrams, and C. E. Wright, "Speed—Accuracy tradeoffs in aimed movements: Toward a theory of rapid voluntary action," in *Attention and Performance XIII*. London, U.K.: Psychology Press, 2018, pp. 173–226.

[47] E. R. F. W. Crossman and P. J. Goodeve, "Feedback control of hand-movement and Fitts' law," *Quart. J. Exp. Psychol. A, Hum. Exp. Psychol.*, vol. 35, no. 2, pp. 251–278, May 1983.